Communication

Active–Passive Reconfigurable Antenna Covering 70–7200 MHz Bandwidth

Shuyu Wang, Zhenyu Liu, Yongjian Zhang, and Yue Li

***Abstract*— This communication presents an active–passive reconfigurable antenna with 70–7200 MHz bandwidth for multiple wireless services. The active–passive reconfiguration is achieved by reusing a properly designed monopole antenna with the active–passive reconfigurable matching circuit, which is composed of a passive path and an active path. The passive path guarantees an inherent bandwidth of 923–7200 MHz for higher frequencies. The active path, achieved by a transistor biased in its ohmic region, ensures the impedance matching within 70–1200 MHz for lower frequencies. The path selection is facilitated by the cooperated design among the transistor, the p-i-n diodes, and their own bias circuits. Therefore, the proposed active–passive reconfigurable antenna achieves a total bandwidth spanning from 70 to 7200 MHz with a reflection coefficient consistently below −10 dB and validated by experiments. Such wideband performance exhibits the exciting potential for multiple-standard signal sensing to support increasing wireless services with a single antenna configuration.**

***Index Terms*— Active antennas, antenna impedance matching, mobile antennas, reconfigurable antennas, wideband antennas.**

I. Introduction

In the face of continually emerging wireless services, the allocated frequencies have expanded across the spectrum [1], [2], [3], [4]. Frequently utilized standards include: frequency modulation (FM) (76–110 MHz), digital television (DTV) (470–770 MHz), global system for mobile communications (GSM) (824–894 MHz), global navigation satellite system (GNSS) (1.2–1.7 GHz), digital communication system (DCS) (1.71–1.88 GHz), universal mobile telecommunication system (UMTS) (1.92–2.17 GHz), wireless local area network (WLAN) (2.4–2.484 GHz, 5.24–5.825 GHz), long term evolution (LTE) (698–787 MHz, 2.3–2.4 GHz, 2.6–2.69 GHz), fifth generation mobile communication technology (5G-Sub 6) (3.3–5 GHz), and Wi-Fi 6E (5.925–7.125 GHz). Therefore, antennas for multiple-standard signal sensing are desperately desirable to cover the entire bandwidth of 70–7200 MHz [5], [6], [7], [8], [9], [10] to support the increasing wireless services.

To realize the possible coverage of the allocated bandwidth, ultra-wideband (UWB) antennas have garnered significant attention in recent decades. Various forms and technologies of UWB antennas have been proposed, encompassing passive UWB antennas [11], [12], [13], [14], [15] and active antennas [16], [17], [18]. For example, the passive UWB antenna proposed in [12] achieves a bandwidth of 3.1–10.6 GHz, whereas the active antenna in [16] covers the 20–110 MHz bandwidth. What is more, the reconfigurable antennas have achieved an ultra-wide tuning range through the use of tunable elements [19], [20], [21]. For instance, the antenna proposed in [20] realizes a bandwidth of 2.5–8.05 GHz. In summary, the entirety of the current proposed UWB antennas only cover a part of the essential bandwidth, leaving the full coverage of 70–7200 MHz still unrealized. Recently, an innovative impedance-matching circuit was proposed for active antennas [22]. This circuit is based on a field-effect transistor (FET) biased in its ohmic region. Utilizing this matching circuit, we have successfully developed an active antenna with coverage from 10 to 1800 MHz, boosting a bandwidth spanning 180 octaves. However, explorations revealed that the operating frequency range of this active antenna is primarily determined by the characteristics of the ohmic FET, posing limitations for achieving other frequency ranges. Therefore, further development is necessary to cover the desired band of 70–7200 MHz.

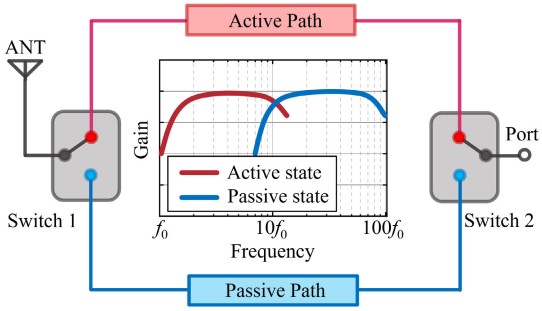

Fig. 1. Conceptual graph of the active–passive reconfigurable antenna.

Here, we present an active–passive reconfigurable antenna with a bandwidth of 70–7200 MHz. The configuration involves reusing a well-designed monopole antenna with an active–passive reconfigurable matching circuit. This matching circuit comprises an active path, a passive path, and a pair of switch modules, as shown in Fig. 1. The active path incorporates the ohmic FET impedance matching circuit proposed in [22], ensuring coverage of the lower frequency band. Constrained by the additional diode control circuits, the antenna covers a bandwidth of 70–1200 MHz via the active path. Conversely, the passive path stimulates the intrinsic bandwidth of 923–7200 MHz for the monopole antenna. Path selection is realized through the switch modules, which are built using p-i-n diodes with control circuits. The geometry of the monopole antenna and the element values are cooperatively designed to achieve an optimized bandwidth. Through this cooperative design process, the active–passive reconfigurable antenna achieves a total bandwidth spanning from 70 to 7200 MHz with a reflection coefficient lower than −10 dB. The reflection coefficients, gains, and radiation patterns of the antenna under active and passive states are simulated and measured. The measurement results align well with the simulated ones, validating the application potential for multiple-standard signal sensing.

II. Active–Passive Reconfigurable Matching Circuit Design

As conceptually depicted in Fig. 1, the proposed active–passive reconfigurable matching circuit consists of an active path, a passive

Manuscript received 10 April 2024; revised 18 June 2024; accepted 5 July 2024. Date of publication 16 July 2024; date of current version 9 September 2024. This work was supported in part by the National Natural Science Foundation of China under Grant U22B2016 and in part by the National Key Research and Development Program of China under Grant 2021YFA0716601. *(Corresponding author: Yue Li.)*

The authors are with the Department of Electronic Engineering, Beijing National Research Center for Information Science and Technology, Tsinghua University, Beijing 100084, China (e-mail: lyee@tsinghua.edu.cn).

Color versions of one or more figures in this article are available at https://doi.org/10.1109/TAP.2024.3426348.

Digital Object Identifier 10.1109/TAP.2024.3426348

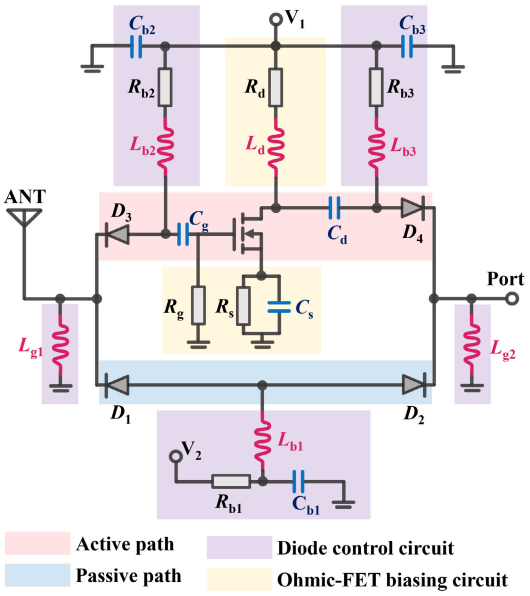

Fig. 2. Circuit diagram of the active–passive reconfigurable antenna.

path, and a pair of switch modules. The diagram of the active–passive reconfigurable matching circuit is depicted and annotated in Fig. 2. Function modules are labeled with different colored frames for clarity. As shown, the red frame designates the active path, in which an ohmic FET has its gate connected to the antenna, and its drain connected to the port. In addition, a pair of capacitors C_g and C_d block the biasing voltages of the ohmic FET and the diodes. The biasing circuit for the ohmic FET is indicated in yellow. The passive path is indicated by a blue frame, representing a microstrip line. The purple frames denote the control circuit of the p-i-n diodes. Each control circuit comprises a choking inductor L_b, a protecting resistor R_b, and a bypass capacitor C_b. Grounding inductors L_{g1} and L_{g2} are reused for both paths. The controlling voltages V_1 and V_2 are incorporated into the biasing circuits to regulate the conducting state of the p-i-n diodes. When diodes D_1 and D_2 are activated, the antenna operates in its passive state. Conversely, when D_3 and D_4 are activated, the antenna functions in its active state. It is worth mentioning that by selecting biasing resistors with appropriate values, the power supply for the diodes and the ohmic FET can be integrated.

We have proposed an active matching method based on an ohmic FET in the previous work [22], achieving a bandwidth of 10–1800 MHz within the size of 30 × 12 × 0.6 mm^3. However, in this matching method, the bandwidth of the active antenna with ohmic FET matching is limited by the FET itself, which makes the antenna size have little effect on its bandwidth. Hence, this ohmic FET matching method cannot be directly applied to cover the essential frequency band from 70 to 7200 MHz. For the effective coverage of this bandwidth, it is necessary to adopt the active–passive reconfigurable matching circuit. However, the introduction of the reconfigurable matching circuit causes a narrower bandwidth compared with the previous active monopole antenna from two aspects. First, a pair of serial p-i-n diodes are connected as serial parasitic inductors in this work, leading to a mismatch at the higher frequencies and thereby limiting the active bandwidth in the high-frequency band. Second, the presence of shunt inductors and the blocking capacitors in the p-i-n diode control circuits deteriorate the low-frequency matching. Therefore, the circuit element values should be elaborately designed to achieve an optimized bandwidth.

TABLE I
ELEMENT VALUES

Element	Value	Element	Value	Element	Value
L_{g1}	270 nH	C_g	68 nF	R_g	10 kΩ
L_{g2}	270 nH	C_s	33 nF	R_s	10 Ω
L_{b1}	135 nH	C_d	68 nF	R_d	120 Ω
L_{b2}	270 nH	C_{b1}	68 nF	R_{b1}	37.5 Ω
L_{b3}	270 nH	C_{b2}	33 nF	R_{b2}	75 Ω
L_d	270 nH	C_{b3}	33 nF	R_{b3}	75 Ω

The steps for determining the values of the matching circuit elements are described here. In this design, a high electron mobility transistor (HEMT) NE3510M04 is used as the ohmic FET. According to the datasheet, the ohmic FET possesses a 50 Ω drain impedance with $V_{GS} = -0.2$ V, $V_{DS} = 0.55$ V, and $I_D = 20$ mA. Therefore, R_g is determined to be 10 kΩ to ensure a 0 V gate voltage. $R_d = 120$ Ω and $R_s = 10$ Ω are chosen, with biasing voltage $V_1 = 3.15$ V to establish this bias point. Choking inductor L_d is 270 nH and bypass inductor C_s is 33 nF. Blocking capacitors C_g and C_d are chosen as 68 nF to minimize the bandwidth deterioration. With the values of the FET biasing elements chosen, the process of determining the values of the reconfigurable matching circuit elements is outlined as follows: First, 270 nH inductors L_{g1} and L_{g2} are utilized to provide a dc ground for the diodes, while choking the ac signal received by the antenna. Second, p-i-n diodes MADP-000907 are utilized in the circuit. According to its datasheet, the p-i-n diodes typically conduct under a basing of 1.3 V and 10 mA. Because the control of the diodes shares the same 3.15 V voltage as the ohmic FET bias, the protecting resistors R_{b2} and R_{b3} are chosen as 75 Ω. Choking inductors L_{b2} and L_{b3} are 270 nH, and bypass capacitors C_{b2} and C_{b3} are 33 nF. Finally, a single circuit controls diodes D_1 and D_2 in the passive path with the protecting resistor R_{b1} of 37.5 Ω. The inductor $L_{b1} = 135$ nH and capacitor $C_{b1} = 68$ nF are also chosen accordingly. The detailed element values are listed in Table I. With this configuration, the antenna operates under its active state with $V_1 = 3.15$ V, and $V_2 = 0$ V, while when $V_1 = 0$ V and $V_2 = 3.15$ V, the antenna operates under its passive state.

III. ANTENNA DESIGN AND SIMULATIONS

In the design process, the geometry of the antenna is firstly designed with full-wave simulation software high-frequency structural simulator (HFSS), which utilizes the finite element method (FEM). In the EM simulation setup, the metal parts are set as perfect electric conductor (PEC) boundary, and an air box with radiation boundary is added. The antenna without circuits is realized with a bandwidth coverage from a lower-edge frequency f_1 to 7200 MHz, as the passive bandwidth. Second, the impedance characteristics of the antenna without circuits are exported and utilized in the circuit simulation. Circuit simulation is conducted with the software Microwave Office, which bases on the method of moments (MOM). The antenna layout is simulated using microstrip lines. The diodes are modeled as a serial resistor when conducted, and a serial capacitor when cut off. As mentioned in [22], the ohmic FET circuit is fabricated and measured, with the S-matrix extracted for circuit simulation. Circuit simulation result yields the bandwidth of the antenna with circuits, as the active bandwidth. The active bandwidth is required to cover the bandwidth from 70 MHz to an upper-edge frequency of f_2, and $f_2 > f_1$ should be achieved to cover the whole bandwidth of 70–7200 MHz. Therefore, the configuration of the antenna is illustrated in Fig. 3, with its top and bottom views depicted in Fig. 4. The detailed geometric parameters of this antenna

TABLE II
GEOMETRIC PARAMETERS (UNIT: MILLIMETERS)

Parameter	r_1	r_2	l_1	l_2	l_3	w	g
Value	24.2	7.1	110	85	32.9	1.3	1.0

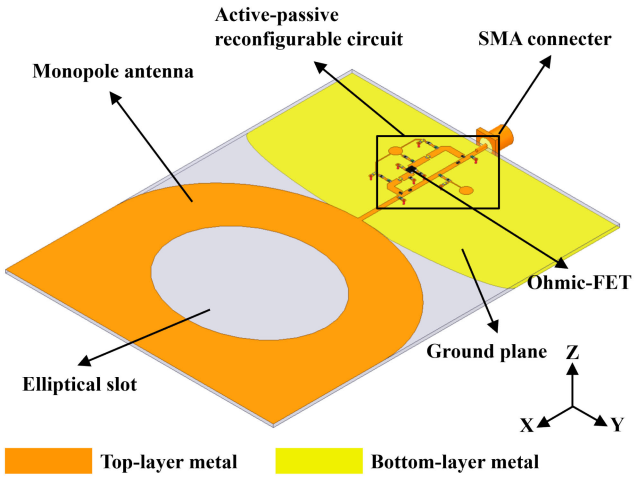

Fig. 3. Perspective view of the active–passive reconfigurable antenna.

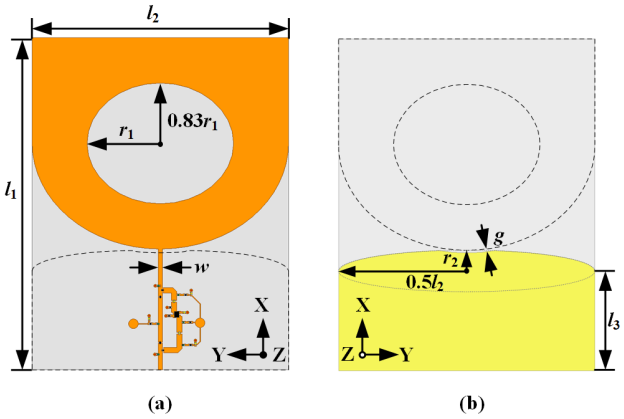

Fig. 4. (a) Top and (b) bottom views of active–passive reconfigurable antenna.

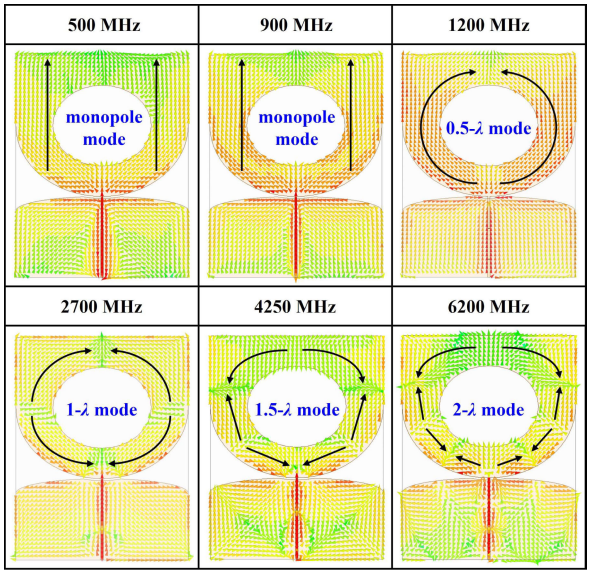

Fig. 5. Simulated current distribution of the monopole antenna under different frequencies.

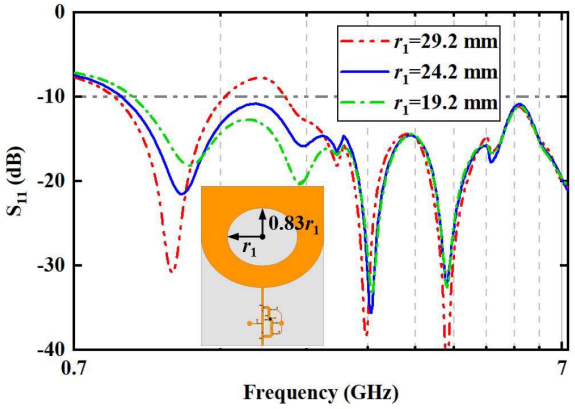

Fig. 6. Simulated passive bandwidth with different values of r_1 and r_2.

are listed in Table II. As shown in Fig. 4, an hourglass-shaped monopole antenna is printed on an FR-4 epoxy substrate ($\varepsilon_r = 4.4$, $\tan\delta = 0.02$) with a thickness of 1 mm. The operating frequency of the antenna without a circuit is dependent on its length l_1, and a suitable frequency is chosen with $l_1 = 110$ mm. An elliptical slot is etched on the monopole for impedance matching. The field distribution of the antenna under different frequencies is illustrated in Fig. 5. Under the active state, the antenna operates at its monopole mode. The antenna is excited with its 0.5-λ mode at 1200 MHz, with its 1-λ, 1.5-λ, and 2-λ modes excited at 2700, 4250, and 6500 MHz, respectively, under the passive state. Therefore, ultrawideband coverage at the passive state is guaranteed. As illustrated in Fig. 6, the impedance of the antenna without circuits is dependent on the size of the slot. Therefore, a matched impedance is realized with a slot with a major radius $r_2 = 24.2$ mm and minor radius $r_1 = 20$ mm. A passive bandwidth from $f_1 = 980$–7200 MHz is thereby realized. It is noteworthy that the antenna also maintains a good matching until 8.6 GHz. The active bandwidth is required to achieve coverage from 70 MHz to f_2, where $f_2 > 980$ MHz. As discussed, the impedance matching under the active state is actualized through configuring the bias point of the FET, which is facilitated by choosing suitable biasing resistors. Simulated active bandwidths with different R_d values are illustrated in Fig. 7, as a demonstration of the effect of R_d on the active bandwidth. As depicted, a matched impedance is realized with $R_d = 120\ \Omega$, corresponding to a bias point where the drain impedance is 50 Ω. On the other hand, altering R_d changes the bias point, causing the drain impedance to deviate from 50 Ω and causing the impedance bandwidth to decrease. Therefore, an active bandwidth of from 70 MHz to $f_2 = 1270$ MHz is realized, fulfilling the requirement of $f_2 > f_1$.

In summary, changing the geometric parameters of the antenna affects its passive bandwidth, while altering the circuit element values influences its active bandwidth. With a cooperative design between the geometry and circuit element values, an antenna covering the bandwidth of 70–7200 MHz is realized. Utilizing the proposed antenna design, the simulated reflection coefficients of the antenna under the active and passive states are illustrated in Fig. 8. The designed antenna possesses an active bandwidth from 70 to 1270 MHz and a passive bandwidth from 980 to 7200 MHz. It is noteworthy that the active bandwidth and passive bandwidth still have a 290-MHz overlap in between. This

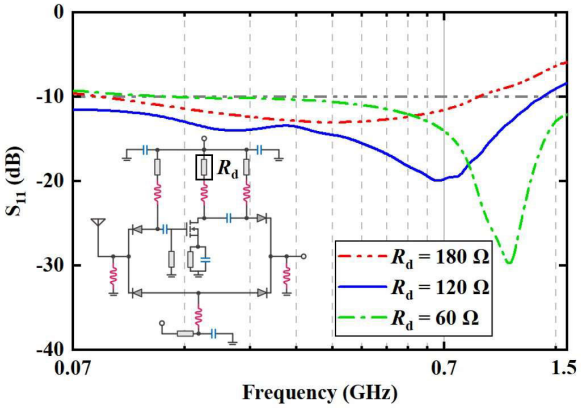

Fig. 7. Simulated active bandwidth with different values of R_d.

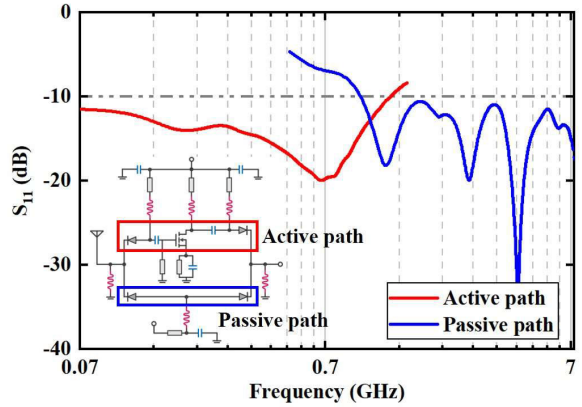

Fig. 8. Simulated active and passive bandwidths of the proposed antenna.

can be further optimized by reducing the size of the antenna, thereby getting a passive bandwidth of higher f_1.

IV. Fabrication and Measurements

A prototype of the active–passive reconfigurable antenna has been fabricated and measured for validation. Fig. 9 illustrates the PCB diagram of the active–passive reconfigurable matching circuit, which occupies a total area of 25 × 25 mm. Fig. 10 shows a photograph of the prototype antenna. The antenna is printed on an FR-4 epoxy substrate with a reconfigurable matching circuit. A pair of solder pads are connected to the dc voltage source, providing biasing voltages V_1 and V_2 for the p-i-n diodes and the ohmic FET. An SMA connecter serves as the feeding port. When the antenna operates under the active state, a voltage of 3.15 V is provided for V_1, while V_2 is set at 0. Under the active state, the antenna employs a dc current of 40 mA, consuming a total dc power of 126 mW. On the other hand, the proposed antenna operates under its passive state when V_2 is 3.15 V and V_1 is 0, with a total dc current of 20 mA and power consumption of 63 mW.

The reflection coefficient of the proposed antenna was characterized with an Agilent N9917A vector network analyzer. The measurement and simulation results are depicted in Fig. 11, revealing good agreement. Measurement results indicate that under the active state, the antenna possesses a bandwidth of 70–1200 MHz, with a reflection coefficient lower than −10 dB. When the antenna operates under the passive state, it covers a bandwidth of 923–7200 MHz. By altering the operation state according to requirements, a total bandwidth of 70–7200 MHz is thereby realized and validated.

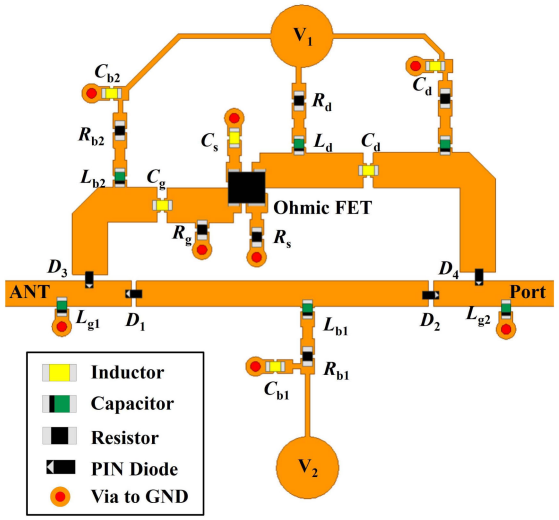

Fig. 9. PCB diagram of the active–passive reconfigurable matching circuit.

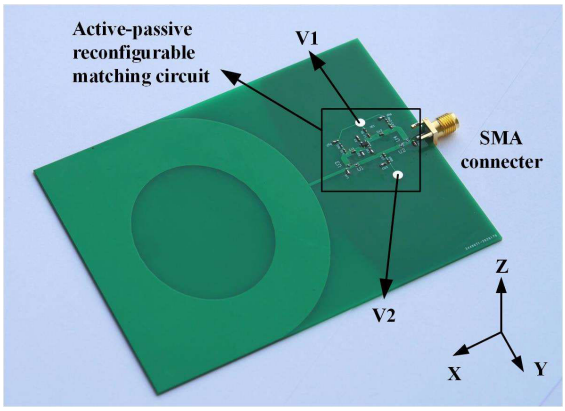

Fig. 10. Photograph of the active–passive reconfigurable antenna.

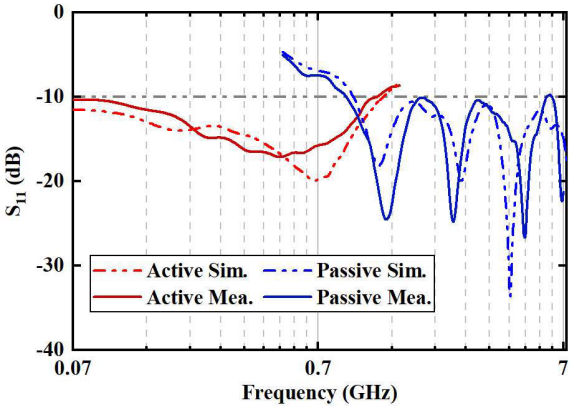

Fig. 11. Simulated and measured reflection coefficient of the active–passive reconfigurable antenna under active and passive states.

The receiving gain of this active–passive reconfigurable antenna is measured in an anechoic chamber. The simulated and measured gains of the proposed antenna under active and passive states are shown in Fig. 12, respectively. The antenna reaches a gain of −6 to 4.4 dBi under the active state. While under the passive state, it has a gain of 0.6–4.88 dBi. Measurement results reveal that active matching introduces obvious gain improvement at the lower frequencies. With active–passive reconfiguration, the antenna

TABLE III
PERFORMANCE COMPARISON

Ref.	Method	B.W.	Vol. (λ_L^2)	Gain (dBi)	Total Efficiency	PAE
[11]	Passive	0.52-1.83 GHz	0.3×0.3	7.2	> 60%	N.A.
[12]	Passive	3.1-10.6 GHz	0.22×0.15	-18.5	N.A.	N.A.
[17]	Active	20-120 MHz	Length: 0.02	5	N.A.	21.1%
[18]	Active	3-22 MHz	Length: 0.02	-10	N.A.	10%
[20]	Reconfigurable	2.5-8.05 GHz	0.29×0.27	4.25	92%	N.A.
[21]	Reconfigurable	6-10.6 GHz	0.86×0.42	3.2	89%	N.A.
[22]	Active	10-1800 Mz	0.001×0.0004	0.85	N.A.	12.8%
This Work	**Active-passive reconfigurable**	**70-7200 MHz**	**0.025×0.02**	**4.88**	**78%**	**18.4%**

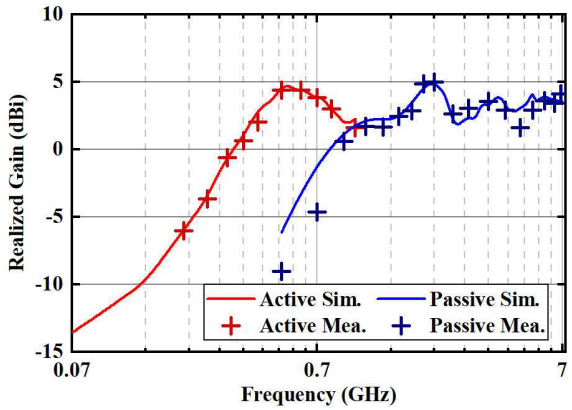

Fig. 12. Simulated and measured realized gain of the active–passive reconfigurable antenna under active and passive states.

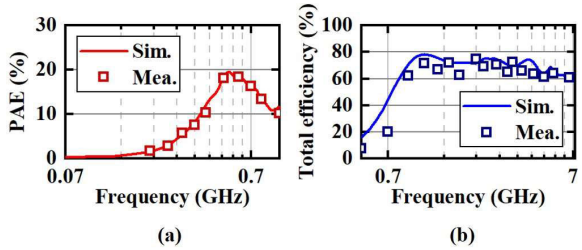

Fig. 13. Simulated and measured results of (a) PAE under active state and (b) total efficiency under passive state.

is proven with a usable gain at lower frequencies, while maintaining high efficiency at the higher frequencies. The simulated and measured results of power-added efficiency (PAE) under the active state, and the total efficiency under the passive state are illustrated in Fig. 13. As depicted, the proposed antenna reaches a peak PAE of 18.8% under the active state, while reaching a peak total efficiency of 78% under the passive state. The simulated and measured radiation patterns are depicted in Fig. 14. The simulated 3-D radiation patterns at 500 and 900 MHz under the active state are illustrated, with the patterns at 1200, 2700, 4250, and 6500 MHz under the passive state. The simulated and measured 2-D radiation patterns at these frequencies and states are illustrated accordingly as verifications. It is notable that at lower frequencies, the reconfigurable antenna exhibits a typical donut-shaped pattern characteristic of a monopole. As the frequency increases, the pattern gradually transforms with emerging sidelobes. Especially, although the radiation pattern is unstable across

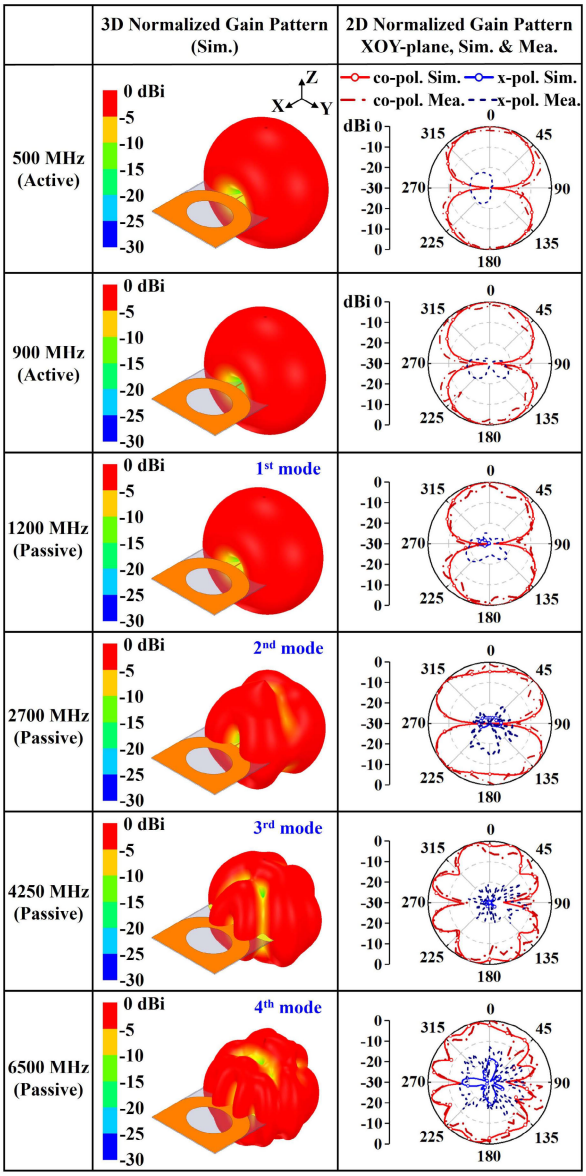

Fig. 14. Three-dimensional and 2-D normalized radiation patterns of the active–passive reconfigurable antenna.

the operating bandwidth, it is acceptable for sensing applications in terminal devices.

To highlight the performance merits of the proposed antenna, Table III summarizes the bandwidth comparison between our work

and other approaches to UWB antenna design. The sizes of the antennas compared to the free-space wavelength corresponding to the lowest operating frequency (denoted λ_L) are also listed. Works [11], [12] succeeded in realizing passive UWB antennas with partial coverage of the essential 70–7200 MHz bandwidth [16], [18] utilize active antennas to achieve wide bandwidth in a small volume. However, their operating frequencies are low, and face the challenge of high-frequency expansion. Works [20], [21] realize an ultrawide bandwidth using compact reconfigurable antennas. Nevertheless, their tuning range is limited, and full coverage of the essential bandwidth is left unrealized. Especially, compared to our previous work [22], this work significantly expands the operating bandwidth at higher frequencies. In summary, the entirety of the state-of-the-art UWB antennas lacks the ability to cover some of the critical bands for wireless services. On the contrary, the active–passive reconfigurable antenna proposed in this work covers a total bandwidth of 70–7200 MHz, encompassing the essential bandwidth of multiple-standard signal sensing.

V. Conclusion

An active–passive reconfigurable antenna is proposed in this communication. In this design, a monopole antenna is reused with an active–passive reconfigurable matching circuit, comprising an active path, a passive path, and a pair of switch modules. The active path is based on the ohmic FET matching technique, providing the antenna with operating ability at lower frequencies. On the other hand, the passive path excites the intrinsic bandwidth of the antenna at higher frequencies. The cooperative design process of this reconfigurable antenna is described in detail. In this process, the geometric parameters of the antenna without a circuit are first determined. Then, the circuit element values are chosen for bandwidth continuity. The antenna geometry defines the passive bandwidth, while circuit element values determine the active bandwidth performance. Simulation and measurement results confirm that the antenna covers a bandwidth of 70–1200 MHz under the active state and a bandwidth of 923–7200 MHz under the passive state. With path selection, the reconfigurable antenna covers a total bandwidth of 70–7200 MHz. Compared to our previous work [22], this antenna breaks the bandwidth limit at higher frequencies and provides an applicable realization of the ohmic FET matching technique. With its wide bandwidth, the active–passive reconfigurable antenna demonstrates application potentials for multiple-standard signal sensing to support the increasing wireless services, including FM, GSM, GNSS, DCS, UMTS, WLAN, LTE, 5G-Sub 6, and Wi-Fi 6E.

References

[1] K.-L. Wong, Y.-C. Lin, and B. Chen, "Internal patch antenna with a thin air-layer substrate for GSM/DCS operation in a PDA phone," *IEEE Trans. Antennas Propag.*, vol. 55, no. 4, pp. 1165–1172, Apr. 2007.

[2] K.-L. Wong and Y.-C. Chen, "Small-size hybrid loop/open-slot antenna for the LTE smartphone," *IEEE Trans. Antennas Propag.*, vol. 63, no. 12, pp. 5837–5841, Dec. 2015.

[3] M. Hu and Y. Li, "Wideband back cover microstrip antenna with multiple shorting vias for mobile 5G MIMO applications," *IEEE Trans. Antennas Propag.*, vol. 71, no. 10, pp. 8290–8295, Oct. 2023.

[4] X. Zhang, D. Zhou, S. Li, Y. Li, K. Wei, and Z. Zhang, "A simple ±45° polarized patch antenna array based on single-sided PCB for Wi-Fi 6/6E application," *IEEE Antennas Wireless Propag. Lett.*, vol. 22, no. 8, pp. 1997–2001, Aug. 2023.

[5] Y. Zhang and Y. Li, "Wideband microstrip antenna in small volume without using fundamental mode," *Electromagn. Sci.*, vol. 1, no. 2, pp. 1–6, Jun. 2023.

[6] C. Mendes and C. Peixeiro, "On-body transmission performance of a novel dual-mode wearable microstrip antenna," *IEEE Trans. Antennas Propag.*, vol. 66, no. 9, pp. 4872–4877, Sep. 2018.

[7] H. Li, Z. Zhou, Y. Zhao, and Y. Li, "Low-loss beam synthesizing network based on Epsilon-near-zero (ENZ) medium for on-chip antenna array," *Chip*, vol. 2, no. 2, Jun. 2023, Art. no. 100049.

[8] Z.-X. Liu, L. Zhu, and N.-W. Liu, "Design approach for compact dual-band dual-mode patch antenna with flexible frequency ratio," *IEEE Trans. Antennas Propag.*, vol. 68, no. 8, pp. 6401–6406, Aug. 2020.

[9] Y. Zhang, Y. Li, W. Zhang, Z. Zhang, and Z. Feng, "Omnidirectional antenna diversity system for high-speed onboard communication," *Engineering*, vol. 11, pp. 72–79, Apr. 2022.

[10] Y. Zhang, Y. Li, M. Hu, P. Wu, and H. Wang, "Dual-band circular-polarized microstrip antenna for ultrawideband positioning in smartphones with flexible liquid crystal polymer process," *IEEE Trans. Antennas Propag.*, vol. 71, no. 4, pp. 3155–3163, Apr. 2023.

[11] X.-Y. Sun et al., "Ultrawideband circularly polarized halved-type Vivaldi antenna with symmetrical radiation pattern," *IEEE Antennas Wireless Propag. Lett.*, vol. 23, no. 2, pp. 633–637, Feb. 2024.

[12] R. Li and Y. Guo, "A conformal UWB dual-polarized antenna for wireless capsule endoscope systems," *IEEE Antennas Wireless Propag. Lett.*, vol. 20, no. 4, pp. 483–487, Apr. 2021.

[13] R. B. V. B. Simorangkir, A. Kiourti, and K. P. Esselle, "UWB wearable antenna with a full ground plane based on PDMS-embedded conductive fabric," *IEEE Antennas Wireless Propag. Lett.*, vol. 17, no. 3, pp. 493–496, Mar. 2018.

[14] L. Y. Nie, X. Q. Lin, Z. Q. Yang, J. Zhang, and B. Wang, "Structure-shared planar UWB MIMO antenna with high isolation for mobile platform," *IEEE Trans. Antennas Propag.*, vol. 67, no. 4, pp. 2735–2738, Apr. 2019.

[15] G. Srivastava and A. Mohan, "Compact MIMO slot antenna for UWB applications," *IEEE Antennas Wireless Propag. Lett.*, vol. 15, pp. 1057–1060, 2016.

[16] S. E. Sussman-Fort, "Matching network design using non-foster impedance," *Int. J. RF Microw. Comput.-Aided Eng.*, vol. 16, pp. 135–143, Feb. 2005.

[17] S. E. Sussman-Fort and R. M. Rudish, "Non-foster impedance matching of electrically-small antennas," *IEEE Trans. Antennas Propag.*, vol. 57, no. 8, pp. 2230–2241, Aug. 2009.

[18] N. Strachen, E. Mohammadi, J. Booske, and N. Behdad, "Active, ultra-wideband, electrically small antennas for high-power transmission in the HF band," *IEEE Trans. Antennas Propag.*, vol. 70, no. 3, pp. 1600–1611, Mar. 2022.

[19] Z. Zhou et al., "Dispersion coding of ENZ media via multiple photonic dopants," *Light, Sci. Appl.*, vol. 11, no. 1, p. 207, Jul. 2022.

[20] M. Gholamrezaei, F. Geran, and R. A. Sadeghzadeh, "Completely independent multi-ultrawideband and multi-dual-band frequency reconfigurable annular sector slot antenna (FR-ASSA)," *IEEE Trans. Antennas Propag.*, vol. 65, no. 2, pp. 893–898, Feb. 2017.

[21] L. Pazin and Y. Leviatan, "Reconfigurable slot antenna for switchable multiband operation in a wide frequency range," *IEEE Antennas Wireless Propag. Lett.*, vol. 12, pp. 329–332, 2013.

[22] S. Wang and Y. Li, "Single-transistor impedance matching circuit for over-hundred-octave active antennas," *IEEE Trans. Antennas Propag.*, vol. 72, no. 3, pp. 2391–2398, Mar. 2024.